Research Article

Humaira Yasmin*, Showkat Ahmad Lone, Ali M. Mahnashi, Waleed Hamali, M. D. Shamshuddin, and Anwar Saeed*

Optimized framework numerical solution for swirling hybrid nanofluid flow with silver/gold nanoparticles on a stretching cylinder with heat source/sink and reactive agents

https://doi.org/10.1515/phys-2023-0202
received November 02, 2023; accepted February 06, 2024

Abstract: The heat and mass transportation for nanofluid across a swirling cylinder under the actions of magnetic effects and Cattaneo–Christov heat flux is reported in the current analysis. The objective of this study is to examine the energy and mass transmissions through hybrid nanofluid under the influence of heat source/sink and reactive species. The hybrid nanoliquid has been prepared by the dispersion of silver (Ag) and gold (Au) nanoparticles (NPs) in the base fluid ethylene glycol ($C_2H_6O_2$). The flow phenomena are expressed in the form of nonlinear partial differential equations and are converted to a nondimensional form, by employing the similarity substitution. For the computational estimation of the problem, the parametric continuation method is employed. The demonstration of velocity, mass, and energy outlines *versus* distinct physical factors is exposed in the form of figures. It has been perceived that the axial and swirling velocity outline drops with the influence of the Reynolds number, magnetic effect, and the insertion of Au and Ag NPs in $C_2H_6O_2$. Furthermore, the hybrid nanofluid energy curve declines with the effect of the Reynolds number, thermal relaxation factor, and the volume friction of NPs.

Keywords: MHD, heat source/sink, Cattaneo–Christov heat flux, spinning cylinder, numerical technique (PCM), hybrid nanofluid flow

*** Corresponding author: Humaira Yasmin,** Department of Basic Sciences, General Administration of Preparatory Year, King Faisal University, Al Ahsa, 31982, Saudi Arabia, e-mail: hhassain@kfu.edu.sa
*** Corresponding author: Anwar Saeed,** Department of Mathematics, Abdul Wali Khan University, Mardan, 23200, Khyber Pakhtunkhwa, Pakistan, e-mail: anwarsaeed769@gmail.com
Showkat Ahmad Lone: Department of Basic Sciences, College of Science and Theoretical Studies, Saudi Electronic University, (Jeddah-M), Riyadh, 11673, Saudi Arabia
Ali M. Mahnashi, Waleed Hamali: Department of Mathematics, College of Science, Jazan University, Jazan, Saudi Arabia
M. D. Shamshuddin: Department of Computer Science and Artificial Intelligence (Mathematics), SR University, Warangal, 506371, Telangana State, India

Nomenclature

ε	uniform rotation
σ_{hnf}	electrical conductivity
ρ_{hnf}	density
(u, v, w)	velocity componenets
C_{w}	surface concentration
k_{hnf}	thermal conductivity
Q_0	internal heat source
δ_{c}	solutal relaxation factor
Re	Reynolds number
M	magnetic parameter
Au	gold
NPs	nanoparticles
PCM	parametric continuation method
a	stretching cylinder
R_1	cylinder radius
B	magnetic field
r	radial direction
μ_{hnf}	dynamic viscosity
T_{w}	surface temperature
D_{B}	mass diffusivity
$(\rho C_{\mathrm{p}})_{\mathrm{hnf}}$	Specific heat
R_{s}	destructive reactive species
δ_{t}	thermal relaxation factor
H	heat source/sink parameter
$C_2H_6O_2$	ethylene glycol
Ag	silver
MHD	magnetohydrodynamics

1 Introduction

The study of hybrid nanofluid flow along an expanding cylinder has gained a great deal of recognition because of its wide range of applications, including glass fiber manufacturing, channel and flyovers in construction management, plastic sheets, paper production, blood transportation, polymer innovation, toxic liquid transport power plants (nuclear), and carriage of dangerous fluids in equipment and machinery [1–3]. Based on their applications in several fields of industries and engineering, a number of researchers have reported on the fluid flow across an elongating cylinder. Bilal *et al.* [4] explored an unsteady fluid flow on a straining cylinder with suction effects. Pattnaik *et al.* [5] described the free convective flow of gold (Au)-based water nanoliquid flow through a channel. Kumar *et al.* [6] examined the energy transportation in hybrid fluid flow on a shrinking sheet using an electrostatic dipole. The results showed that an intensification in the magnetization interaction diminishes the velocity curve, but an opposite pattern is observed in the concentration and energy outlines. Alhowaity *et al.* [7] numerically reviewed the Williamson hybrid nanoliquid flow with heat characteristics across a prolonging surface. Abbasi *et al.* [8] used Fe_3O_4 and Cu in blood to explore thermal transportation inside a curved wavy conduit with slip constraints. Pattnaik *et al.* [9] presented the theoretical approach for catalytic aggressive species propagation in an axisymmetric covering that incorporates forced convection flow from a linear fashion elongating perpendicular cylinder dipped in a homogeneous non-Darcy permeable medium filled with magnetic ferrofluid. Ramzan *et al.* [10] proceeded the detail about the outcome of the heat generator on the nanocomposite flow over an extending cylinder and sheet. The Burger nanoliquid factor and Deborah number were found to lessen nanofluid velocity in both the shrinking cylinder and sheet. Seid *et al.* [11] presented a mathematical framework for analyzing the slip properties on an electrically charged nanoliquid flow over an upward swelling surface. Raising the velocity slip factor accelerates the flow velocity, while enhancing the Soret influence boosts the concentration of nanomaterials near the shrinking sheet. Recently, numerous researchers have presented findings on the fluid flow over an elongated cylinder [12–15].

Hybrid nanofluids are a novel form of fluids formed by scattering nanometer-sized components in base fluids (nanofibers, nanoparticles (NPs), nanowires, nanorods, nanotubes, droplets, or nanosheets). Nanofluids, in another phrase, are nanosized colloidal suspensions comprising concentrated nanocomposites. When compared with conventional fluids such as water and oil, nanoliquids have improved thermophysical characteristics such as dissipation factor, thermal conductivity, convective heat transfer, and viscosity. It has demonstrated a promising potential in a variety of disciplines [16–18]. In the current analysis, we are using silver (Ag) and Au NPs in ethylene glycol. Unique optical characteristics of nanofluids (nanofluids-based microbial fuel cell, nanofluids as vehicular brake fluids, and intensify microreactors), biomedical applications (nanodrug delivery, antibacterial activity), mechanical applications (magnetic sealing, friction reduction, solar absorption, energy storage), and mass and heat transfer intensification (space and defense, nuclear systems cooling, heating buildings and reducing pollution, industrial cooling applications, transportation, and electronic applications) are some uses and applications of the Au-Ag/$C_2H_6O_2$-based nanofluid [19–21]. Bilal *et al.* [22] used the bvp4c package and the parametric continuation method (PCM) technique to numerically simulate carbon nanotubes and microorganisms' water-based nanoliquid flow influenced by a curly fluctuating rotating plate with heat dissemination. Alharbi *et al.* [23] revealed the nanofluid flow with energy transfer containing metallic NPs across an elongated cylinder with magnetization impacts. It was exposed that the Prandtl magnetic number upshot drops the flow velocity, while boosting the energy resume. Zhang *et al.* [24] explored the 3D flow across a circular cylinder of varying surface area and the modified Fourier law. The efficiency of the hybrid-nanoliquid was found to be far superior to that of the conventional ferrofluid. Akram *et al.* [25] evaluated the peristaltically controlled electro-osmotic stimulation of Ag–Au/water-based hybrid nanofluids across a highly permeable inclined nonsymmetric fluid flow. It was renowned that the hybrid nanoliquid allows a more efficient heat transmission rate than silver—water, and thermodynamic premises are significantly advanced in the instance of hybrid nanofluids. Sreedevi *et al.* [26] quantitatively analyzed the Ag- and water-based convective fluid flow within a square cavity with isothermal and adiabatic conditions, while considering magnetic influence. When 0.05% of Ag NPs are dissolved in water, the rate of energy transport increases up to 12.4% from 6.3%. Waqas *et al.* [27] documented the significance of Ag–Au NPs submerged in the base fluid (human blood) and revealed that enhancing the behavior of the thermal radiation and Biot number increases the energy transmission rate. Nanda *et al.* [28] inspected the hybrid nanofluid flow and thermal escalation of a nonlinear extended sheet. When compared to a smooth surface, the curly pivoting substrate enhances heat transfer up to 15%. Studies on the Ag–Au-based nanofluid and hybrid nanofluid may be found in some recent literature [21,29–32].

The significance of magnetohydrodynamics (MHD) can be found in astrophysics, geophysics, engineering, pointing, and sensing magnetic drug. MHD fluid flow

overcomplicated geometry, which is engaged in human body components in addition to commercial applications, is an attractive and important scientific subject [33–35]. Bejawada *et al.* [36] offered a computational examination of MHD nanofluid flow through a nonlinear slanted extending surface. Kodi and Mopuri [37] used a Soret-aligned chemical reaction and a magnetic field to simulate the volumetric flow on an elevated sheet. The existence of an aligned magnetic field and Casson fluid characteristics are said to have a velocity detrimental influence. Mahabaleshwar *et al.* [38] scrutinized the MHD nanofluid flow in the context of mass dissipation and heat conduction. It was discovered that the induced magnetic field improves skin surface friction and decreases surface mass transport, and this was documented in the literature [31,39–45].

The determination in the present research is to examine the heat and mass transport through hybrid nanoliquid across a swirling cylinder under the impact of magnetic effects and Cattaneo–Christov heat flux. The energy and mass communications are also calculated under the effects of heat source/sink and reactive species. The nanoliquid has been produced by the dispersion of Ag and Au-NPs in the base fluid ($C_2H_6O_2$). For the numerical estimation of the problem, the PCM approach is used.

2 Mathematical formulation of the problem

The developed axisymmetric 3D mathematical model under the flow assumptions on a stretching cylinder is deliberated (Figure 1). The flow is produced due to the uniform stretching and rotation of the cylinder with radius R_1, which is immersed in a hybrid nanofluid containing Ag and Au solid NPs. Here, z direction is along the axis of the cylinder, where r is the radial direction. The magnetic effect $B = (0, 0, B_0)$ is functional perpendicular to the cylinder. T_w, C_w are surface and T_∞, C_∞ are temperature and concentration at free stream, where T_w, T_∞, $C_w > C_\infty$ By using the aforementioned presumptions, the modeled equations are expressed as follows [46,47]:

$$(w)_r + (u)_z + \frac{w}{r} = 0, \tag{1}$$

$$w(w)_r + u(u)_z = \frac{\mu_{\mathrm{hnf}}}{\rho_{\mathrm{hnf}}}\left\{(u)_{rr} + \frac{1}{r}(u)_r\right\} - \frac{\sigma_{\mathrm{hnf}}B_0^2}{\rho_{\mathrm{hnf}}}u, \tag{2}$$

$$u(v)_z + w(v)_r + \frac{vw}{r} = \frac{\mu_{\mathrm{hnf}}}{\rho_{\mathrm{hnf}}}\left\{(v)_{rr} - \frac{v}{r^2} + \frac{1}{r}(v)_r\right\} - \frac{\sigma_{\mathrm{hnf}}B_0^2}{\rho_{\mathrm{hnf}}}v, \tag{3}$$

$$\begin{aligned} w(T)_r + u(T)_z \;=\; & \alpha_{\mathrm{hnf}}\left\{(T)_{rr} + \frac{1}{r}(T)_r\right\} \\ & - \lambda_t\{u^2(T)_{zz} + w^2(T)_{rr} + 2uw(T)_{zr} \\ & \quad + w(u)_r(T)_z + u(T)_z(u)_z \\ & + w(w)_r(T)_r + (T)_r u(w)_z\} \\ & + \frac{Q_0}{(\rho C_{\mathrm{p}})_{\mathrm{hnf}}}(T - T_\infty) \\ & + \lambda_{\mathrm{t}}\frac{Q_0}{(\rho C_{\mathrm{p}})_{\mathrm{hnf}}}\{w(T)_z + u(T)_z\}, \end{aligned} \tag{4}$$

$$\begin{aligned} w(C)_r\, u(C)_z \;=\; & D_{\mathrm{B}}\left\{(C)_{rr} + \frac{1}{r}(C)_r\right\} \\ & - \lambda_{\mathrm{c}}\{u^2(C)_{zz} + w^2(C)_{rr} + 2uw(C)_{zr} \\ & + w(u)_r(C)_z + (C)_z u(u)_z \\ & + w(w)_r(C)_r + (C)_r u(w)_z\} \\ & - k_{\mathrm{c}}(C - C_\infty) - k_{\mathrm{c}}\lambda_{\mathrm{c}}\{w(C)_z + u(C)_z\}. \end{aligned} \tag{5}$$

The constraints at boundary are as follows:

$$\left.\begin{array}{l} \text{at } r = R_1 :\; u = 2az,\;\; v = E,\;\; w = 0,\;\; T = T_w,\;\; C = C_w, \\ \text{as } r \to \infty :\; u \to 0,\; v \to 0,\;\; T \to T_\infty,\;\; C \to C_\infty \end{array}\right\}. \tag{6}$$

Here, (u,v,w) denote velocity componenets. Dynamic viscosity of nanoliquid μ_{hnf}, density ρ_{hnf}, electrical conductivity σ_{hnf}, thermal conductivity k_{hnf}, specific heat $(\rho C_{\mathrm{p}})_{\mathrm{hnf}}$, magnetic field strength B_0, energy and mass relaxation time conveyance, respectively, are $(\lambda_{\mathrm{t}}, \lambda_{\mathrm{c}})$, mass diffusivity D_{B}, and internal heat source Q_0.

The attributes of nondimensional terms are as follows:

$$\left.\begin{array}{l} \eta = \dfrac{r^2}{R_1^2},\;\; u = 2azf'(\eta),\;\; v = Eh(\eta), \\ w = \dfrac{-aR_1 f(\eta)}{\eta^{1/2}},\;\; \theta(\eta) = \dfrac{T - T_\infty}{T_w - T_\infty},\;\; \varphi(\eta) = \dfrac{C - C_\infty}{C_w - C_\infty} \end{array}\right\}. \tag{7}$$

When Eq. (7) is applied on Eqs. (1)–(6), we obtain

$$\frac{N_1}{N_2}\left(\frac{1}{\eta}f'' + f'''\right) + \frac{\mathrm{Re}}{\eta}\left(f''f - f' - \frac{1}{2}\frac{N_5}{N_2}Mf'\right) = 0, \tag{8}$$

$$\frac{N_1}{N_2}\left(2\eta^2 h'' + 2\eta h' - \frac{h}{2}\right) + \mathrm{Re}\eta\left(2fh' + \frac{1}{\eta}fh - \frac{N_5}{N_4}Mh\right) = 0, \tag{9}$$

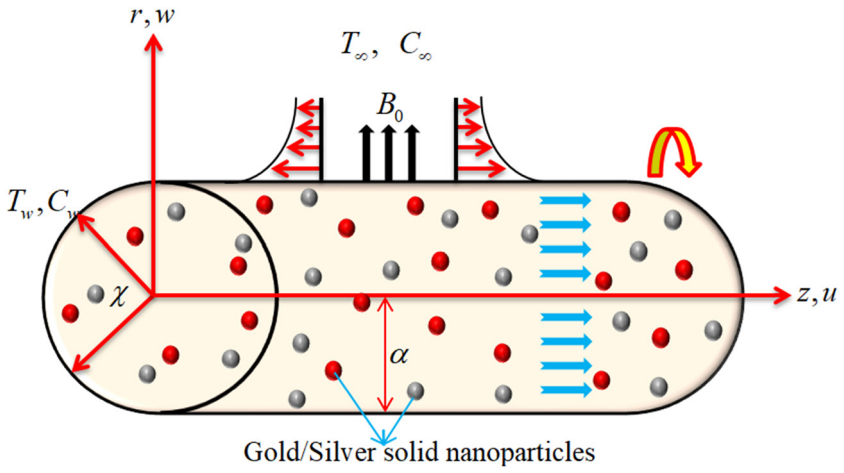

Figure 1: Flow configuration model.

$$(\eta\theta'' + \theta') - 2\delta_t\frac{N_3}{N_4}\mathrm{Re\,Pr}(\theta'' f^2 + ff'\theta') + \frac{\mathrm{Re\,Pr}}{N_4}\left(\frac{H}{2}\theta + N_3 f\theta'\right) = 0, \tag{10}$$

$$\eta\varphi'' + \varphi' - 2\delta_c\mathrm{RePrLe}(\varphi'' f^2 + f\varphi' f') + \mathrm{RePrLe}\left(f\varphi' - \frac{R_s}{2}\varphi\right) = 0. \tag{11}$$

With the transformed boundary conditions,

$$\left.\begin{aligned} &f'(1) = 1,\ f(1) = 0,\ h(1) = 1,\ \theta(1) = 1,\ \varphi(1) = 1,\\ &f'(\infty) \to 0,\ h(\infty) \to 0,\ \theta(\infty) \to 0,\ \varphi(\infty) \to 0. \end{aligned}\right\} \tag{12}$$

Re = $aR_1^2/2\nu$ is the Reynolds number, $M = \sigma_{\mathrm{bf}}B_0^2/\rho_{\mathrm{bf}}a$ indicates the magnetic parameter, $\mathrm{Pr} = \nu/\alpha_{\mathrm{bf}}$ indicates the Prandtl number, $H = Q_0/a(\rho C_{\mathrm{p}})_{\mathrm{bf}}$ indicates the heat source/sink parameter, $\mathrm{Le} = \frac{\alpha_1}{D_B}$ is the Lewis number, $\delta_t = a\lambda_t$ represents the thermal relaxation factor, $\delta_c = a\lambda_c$ represents the solutal relaxation factor, and $R_s = k_c/a$ point out destructive reactive species.

Now for the nanofluids [48], let us present the following expression for μ_{hnf}, ρ_{hnf}, $(\rho C_{\mathrm{p}})_{\mathrm{hnf}}$, k_{hnf}, and σ_{hnf} as follows:

$$\begin{aligned}
&\frac{\mu_{\mathrm{hnf}}}{\mu_{\mathrm{bf}}} = \frac{1}{(1-\phi_{\mathrm{Au}}-\phi_{\mathrm{Ag}})^{2.5}},\quad \frac{\rho_{\mathrm{hnf}}}{\rho_{\mathrm{bf}}} = \phi_{\mathrm{Au}}\left(\frac{\rho_{\mathrm{Au}}}{\rho_{\mathrm{bf}}}\right) + \phi_{\mathrm{Ag}}\left(\frac{\rho_{\mathrm{Ag}}}{\rho_{\mathrm{bf}}}\right) + (1-\phi_{\mathrm{Au}}-\phi_{\mathrm{Ag}}),\\
&(\rho C_{\mathrm{p}})_{\mathrm{hnf}} = \phi_{\mathrm{Au}}\left(\frac{(\rho C_{\mathrm{p}})_{\mathrm{Au}}}{(\rho C_{\mathrm{p}})_{\mathrm{bf}}}\right) + \phi_{\mathrm{Ag}}\left(\frac{(\rho C_{\mathrm{p}})_{\mathrm{Ag}}}{(\rho C_{\mathrm{p}})_{\mathrm{bf}}}\right) + (1-\phi_{\mathrm{Au}}-\phi_{\mathrm{Ag}}),\\
&\frac{k_{\mathrm{hnf}}}{k_{\mathrm{bf}}} = \left[\frac{\left(\frac{\phi_{\mathrm{Au}}k_{\mathrm{Au}}+\phi_{\mathrm{Ag}}k_{\mathrm{Ag}}}{\phi_{\mathrm{Au}}+\phi_{\mathrm{Ag}}}\right) + 2k_{\mathrm{bf}} + 2(\phi_{\mathrm{Au}}k_{\mathrm{Au}}+\phi_{\mathrm{Ag}}k_{\mathrm{Ag}}) - 2(\phi_{\mathrm{Au}}+\phi_{\mathrm{Ag}})k_{\mathrm{bf}}}{\left(\frac{\phi_{\mathrm{Au}}k_{\mathrm{Au}}+\phi_{\mathrm{Ag}}k_{\mathrm{Ag}}}{\phi_{\mathrm{Au}}+\phi_{\mathrm{Ag}}}\right) + 2k_{\mathrm{bf}} - 2(k_{\mathrm{Au}}\phi_{\mathrm{Au}}+k_{\mathrm{Ag}}\phi_{\mathrm{Ag}}) + 2(\phi_{\mathrm{Au}}+\phi_{\mathrm{Ag}})k_{\mathrm{bf}}}\right],\\
&\frac{\sigma_{\mathrm{hnf}}}{\sigma_{\mathrm{bf}}} = \left[\frac{\left(\frac{\phi_{\mathrm{Au}}\sigma_{\mathrm{Au}}+\sigma_{\mathrm{Ag}}\phi_{\mathrm{Ag}}}{\phi_{\mathrm{Ag}}+\phi_{\mathrm{Au}}}\right) + 2\sigma_{\mathrm{bf}} - 2(\phi_{\mathrm{Au}}+\phi_{\mathrm{Ag}})\sigma_{\mathrm{bf}} + 2(\sigma_{\mathrm{Au}}\phi_{\mathrm{Au}}+(\phi_{\mathrm{Ag}})\sigma_{\mathrm{Ag}})}{\left(\frac{\phi_{\mathrm{Au}}\sigma_{\mathrm{Au}}+\phi_{\mathrm{Ag}}\sigma_{\mathrm{Ag}}}{\phi_{\mathrm{Au}}+\phi_{\mathrm{Ag}}}\right) + 2\sigma_{\mathrm{bf}} + \sigma_{\mathrm{bf}}(\phi_{\mathrm{Au}}+\phi_{\mathrm{Ag}}) - (\sigma_{\mathrm{Au}}\phi_{\mathrm{Au}}+(\phi_{\mathrm{Ag}})\sigma_{\mathrm{Ag}})}\right].
\end{aligned} \tag{13}$$

The nanofluid constants can be stated as follows:

$$N_1 = \frac{\mu_{\mathrm{hnf}}}{\mu_{\mathrm{bf}}},\quad N_2 = \frac{\rho_{\mathrm{hnf}}}{\rho_{\mathrm{bf}}},\quad N_3 = \frac{(\rho C_{\mathrm{p}})_{\mathrm{hnf}}}{(\rho C_{\mathrm{p}})_{\mathrm{bf}}}, N_4 = \frac{k_{\mathrm{hnf}}}{k_{\mathrm{bf}}},\quad N_5 = \frac{\sigma_{\mathrm{hnf}}}{\sigma_{\mathrm{bf}}}. \tag{14}$$

The thermophysical features of nanoliquid are presented in Table 1.

Eqs. (8)–(11) are valid only for values (>0) of Re and slow convergence as disclosed by Fang and Yao [49]. So, further transformations $\eta = e^x$ is used to quicken the approach of the solutions, which lead to the following equations:

$$\frac{N_1}{N_2}(f_{xxx} - 2f_{xx} + f_x) - \mathrm{Re}\left(f_x^2 + ff_x - ff_{xx} - \frac{1}{2}\frac{N_5}{N_2}Mf_x e^x\right) = 0, \tag{15}$$

$$2\frac{N_1}{N_2}h_{xx} - \frac{h}{2} + \mathrm{Re}\left(2fh_x + fh - \frac{N_5}{N_4}Mhe^x\right) = 0, \tag{16}$$

$$\theta_{xx}e^x - 2\delta_t\frac{N_3}{N_4}\mathrm{Re\ Pr}(\theta_{xx}f^2 - \theta_x f^2 + ff_x\theta_x) + \frac{\mathrm{Re\ Pr}}{N_4}\left(e^{-2x}\frac{H}{2}\theta + N_3 f\theta_x e^x\right) = 0, \tag{17}$$

$$\varphi_{xx}e^x - 2\delta_c\mathrm{Re\ Le}(f^2\varphi_{xx} - f^2\varphi_x + ff_x\varphi_x)\mathrm{Pr} + \mathrm{Re\ Le}\left(f\varphi_x e^x - \frac{R_s}{2}\varphi\right)\mathrm{Pr} = 0. \tag{18}$$

Along with transformed boundary conditions

$$\left.\begin{aligned} &f(0) = 0,\ f_x(0) = 1,\ h(0) = 1,\ \ \theta(0) = 1,\ \ \varphi(0) = 1,\\ &\lim_{x\to\infty} e^x f_x = 0,\ \ h(\infty) = 0,\ \ \theta(\infty) = 0,\ \varphi(\infty) = 0 \end{aligned}\right\}. \tag{19}$$

The physical quantities local surface friction C_f, Nusselt number Nu_x, and Sherwood number Sh_x are mathematically given as follows:

$$\begin{aligned} \mathrm{Re}^{-1/2}C_{f_z} &= \frac{1}{(1-\phi_{Au}-\phi_{Ag})^{2.5}}f''(0),\\ \mathrm{Re}^{-1/2}C_{g_r} &= \frac{1}{(1-\phi_{Au}-\phi_{Ag})^{2.5}}h'(0), \end{aligned} \tag{20}$$

$$\mathrm{Nu}_z = -2\theta'(1), \tag{21}$$

$$\mathrm{Sh}_x = -2\phi'(1). \tag{22}$$

3 Numerical solution

The detailed description regarding the PCM methodology is as follows [50–53]:

Step 1: Generalization to first-order ordinary differential equation

$$\left.\begin{aligned} &\lambda_1(\eta) = f(\eta),\ \lambda_3(\eta) = f''(\eta),\ \lambda_5(\eta) = h'(\eta),\\ &\lambda_7(\eta) = \theta'(\eta),\ \lambda_9(\eta) = \varphi'(\eta),\\ &\lambda_2(\eta) = f'(\eta),\ \lambda_4(\eta) = h(\eta),\ \lambda_6(\eta) = \theta(\eta),\\ &\lambda_8(\eta) = \varphi(\eta). \end{aligned}\right\}. \tag{23}$$

By setting Eq. (23) in Eqs. (15)–(18) and (19), we obtain:

$$\frac{N_1}{N_2}(\lambda'_3 - 2\lambda_3 + \lambda_2) - \mathrm{Re}\left(\lambda_2^2 + \lambda_1\lambda_2 - \lambda_1\lambda_3 - \frac{1}{2}\frac{N_5}{N_2}M\lambda_2 e^x\right) = 0, \tag{24}$$

$$2\frac{N_1}{N_2}\lambda'_5 - \frac{\lambda_4}{2} + \mathrm{Re}\left(2f\lambda_5 + f\lambda_4 - \frac{N_5}{N_4}M\lambda_4 e^x\right) = 0, \tag{25}$$

$$\lambda'_7 e^x - 2\delta_t\frac{N_3}{N_4}\mathrm{RePr}(\lambda_1^2\lambda'_7 - \lambda_1^2\lambda_7 + \lambda_1\lambda_2\lambda_7) + \frac{\mathrm{RePr}}{N_4}\left(e^{-2x}\frac{H}{2}\lambda_6 + N_3\lambda_1\lambda_7 e^x\right) = 0, \tag{26}$$

$$\lambda'_9 e^x - 2\delta_c\mathrm{ReLe}(\lambda_1^2\lambda'_9 - \lambda_1^2\lambda_9 + \lambda_1\lambda_2\lambda_9)\mathrm{Pr} + \mathrm{ReLe}\left(\lambda_1\lambda_9 e^x - \frac{R_s}{2}\lambda_8\right)\mathrm{Pr} = 0. \tag{27}$$

Along with transformed boundary conditions

$$\left.\begin{aligned} &\lambda_1(0) = 0,\ \lambda_2(0) = 1,\ \lambda_4(0) = 1,\ \ \lambda_6(0) = 1,\\ &\lambda_8(0) = 1,\\ &\lim_{x\to\infty} e^x\lambda_2 = 0,\ \ \lambda_4(\infty) = 0,\ \ \lambda_6(\infty) = 0, \lambda_8(\infty) = 0 \end{aligned}\right\} \tag{28}$$

Step 2: Introducing parameter p in Eqs. (24)–(27)

$$\frac{N_1}{N_2}(\lambda'_3 - 2(\lambda_3 - 1)p + \lambda_2) - \mathrm{Re}\left(\lambda_2^2 + \lambda_1\lambda_2 - \lambda_1\lambda_3 - \frac{1}{2}\frac{N_5}{N_2}M\lambda_2 e^x\right) = 0, \tag{29}$$

$$2\frac{N_1}{N_2}\lambda'_5 - \frac{\lambda_4}{2} + \mathrm{Re}\left(2f(\lambda_5 - 1)p + f\lambda_4 - \frac{N_5}{N_4}M\lambda_4 e^x\right) = 0, \tag{30}$$

$$\lambda'_7 e^x - 2\delta_t\frac{N_3}{N_4}\mathrm{RePr}(\lambda_1^2\lambda'_7 - \lambda_1^2(\lambda_7 - 1)p + \lambda_1\lambda_2\lambda_7) + \frac{\mathrm{RePr}}{N_4}\left(e^{-2x}\frac{H}{2}\lambda_6 + N_3\lambda_1\lambda_7 e^x\right) = 0, \tag{31}$$

$$\lambda'_9 e^x - 2\delta_c\mathrm{ReLe}(\lambda_1^2\lambda'_9 - \lambda_1^2(\lambda_9 - 1)p + \lambda_1\lambda_2\lambda_9)\mathrm{Pr} + \mathrm{ReLe}\left(\lambda_1\lambda_9 e^x - \frac{R_s}{2}\lambda_8\right)\mathrm{Pr} = 0, \tag{32}$$

$$\left.\begin{aligned} &\lambda_1(0) = 0,\ \lambda_2(0) = 1,\ \lambda_4(0) = 1,\ \ \lambda_6(0) = 1,\\ &\lambda_8(0) = 1,\\ &\lim_{x\to\infty} e^x\lambda_2 = 0,\ \ \lambda_4(\infty) = 0,\ \ \lambda_6(\infty) = 0,\ \lambda_8(\infty) = 0 \end{aligned}\right\}. \tag{33}$$

Step 3: Solving the Cauchy problems
By using implicit numerical scheme:

Table 1: Following [48], thermo-physical properties of nanoparticulates with base fluid

Properties	Base fluid	NPs	
	$C_2H_6O_2$ (ethylene glycol)	Ag	Au
ρ(Kg m^{-3})	1,115	10,500	19,300
c_p(J Km^{-1} m^{-1})	2,430	235	129.1
k(W m^{-1} K^{-1})	0.253	429	318
$\beta \times 10^{-5}$ (K^{-1})	5.7	1.89	1.4
σ(S m^{-1})	10.7×10^{-5}	6.30×10^{7}	4.25×10^{7}

Table 2: The comparison of the present results *versus* the existing study for $h'(1)$ and $f''(1)$ by taking $M = H = 0$.

Re	Fang and Yao [49] $f''(1)$	Jawad *et al.* [47] $f''(1)$	Present study $f''(1)$	Fang and Yao [49] $h'(1)$	Jawad *et al.* [47] $h'(1)$	Present study $h'(1)$
0.1	−0.48170	−0.48950	−0.489523	−0.51018	−0.51022	−0.510242
0.2	−0.61738	−0.61415	−0.614163	−0.52604	−0.52740	−0.527463
0.5	−0.88210	−0.88602	−0.886048	−0.58487	−0.58561	−0.585634
1.0	−1.17765	−1.17940	−1.179428	−0.68771	−0.687933	−0.687947
2.0	−1.59379	−1.59600	−1.596023	−0.87262	−0.87263	−0.872662
5.0	−2.41733	−2.41788	−2.417967	−1.29787	−1.29787	−1.297972
10	−3.34436	−3.34444	−3.344673	−1.81005	−1.81006	−1.810281

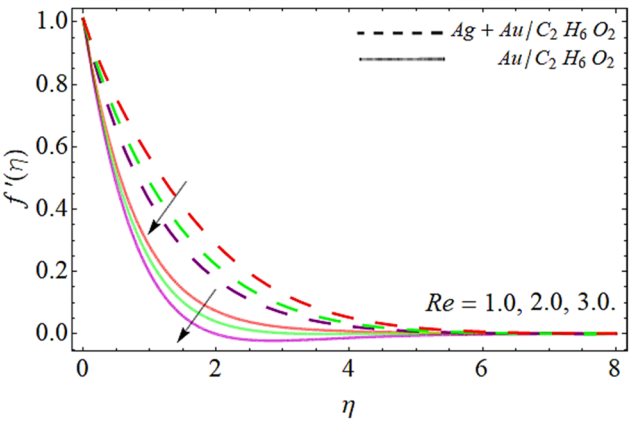

Figure 2: Performance of axial velocity curve $f'(\eta)$ *versus* the Reynolds number Re.

$$\frac{U^{i+1} - U^i}{\Delta\eta} = \mathrm{AU}^{i+1} \text{ and } \frac{W^{i+1} - W^i}{\Delta\eta} = AW^{i+1}. \quad (34)$$

The final iterative form is attained as follows:

$$U^{i+1} = \frac{U^i}{(I - \Delta\eta A)} \text{ and } W^{i+1} = \frac{(W^i + \Delta\eta R)}{(I - \Delta\eta A)}. \quad (35)$$

3.1 Validation of the results

For the validity of the present results, the obtained numerical results for skin friction are related to the published work as shown in Table 2. It can be observed that the present results have greater similarity with the published studies.

4 Results and discussion

This section revealed the physics behind the graphical results. For the velocity energy and mass outlines, we have used the following default values of parameters:
Re = 1, M = 2, Pr = 6.2, $\phi_1 = \phi_2 = 0.02$,
Le = 1, H = 1.5, R_s = 1.5, δ_t = 0.1, δ_c = 0.1.

4.1 Velocity interpretations

Figures 2–4 exhibit the appearance of the axial velocity curve $f'(\eta)$ against the Reynolds number Re, magnetic effect M and NPs. Figure 2 testifies that the velocity panel drops

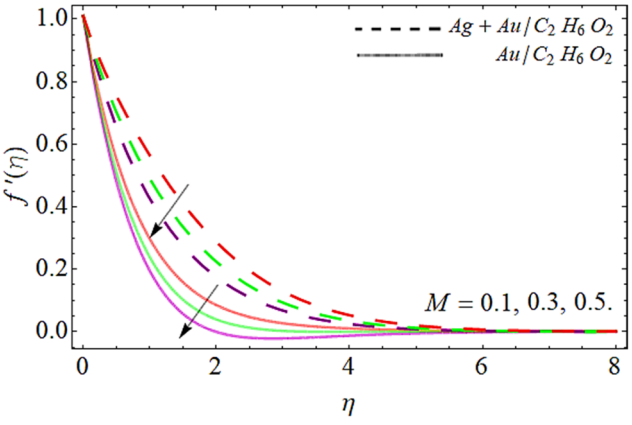

Figure 3: Performance of axial velocity curve $f'(\eta)$ *versus* the magnetic effect M.

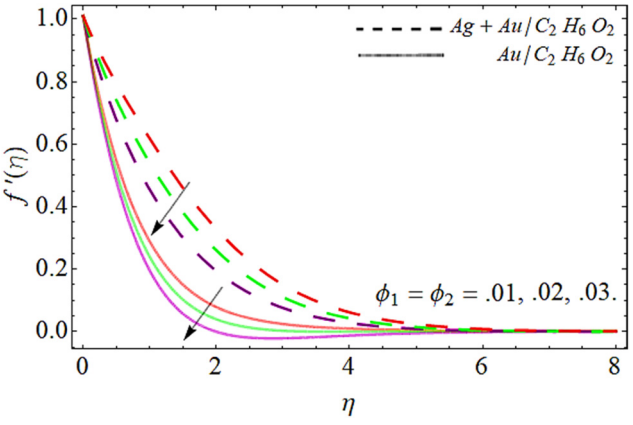

Figure 4: Performance of axial velocity curve $f'(\eta)$ *versus* NPs volume friction.

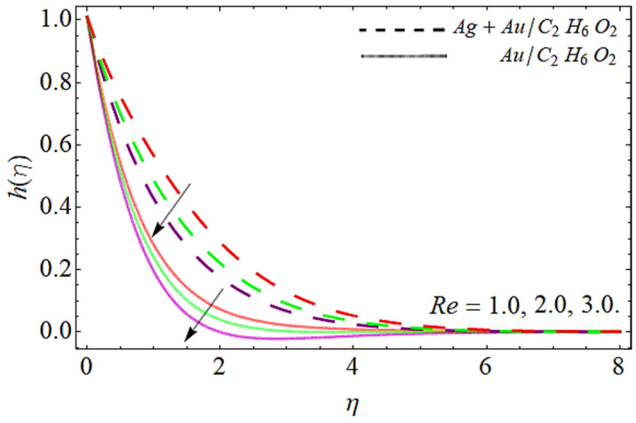

Figure 5: Performance of swirling curve $h(\eta)$ *versus* the Reynolds number Re.

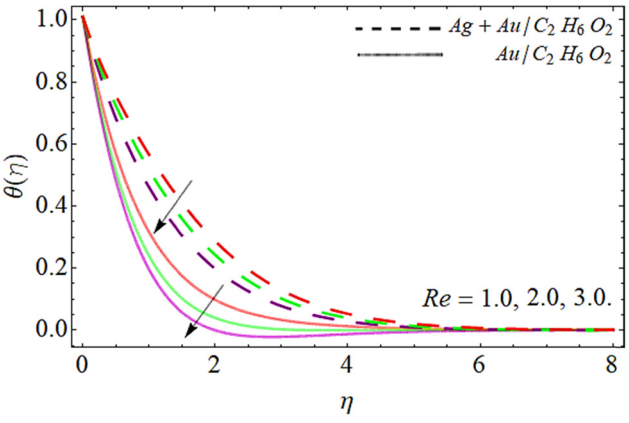

Figure 8: Performance of energy curve $\theta(\eta)$ *versus* the Reynolds number Re.

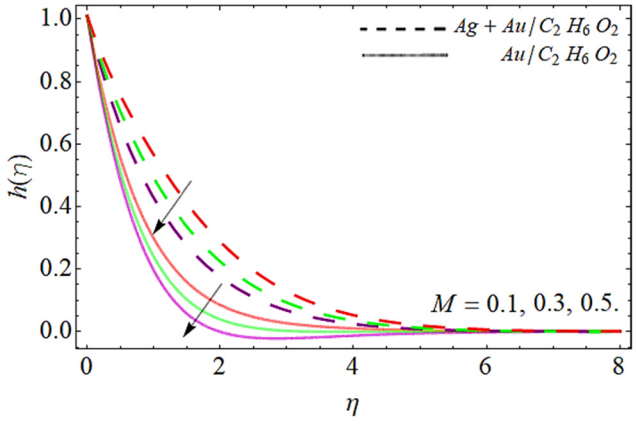

Figure 6: Performance of swirling curve $h(\eta)$ *versus* the magnetic effect *M*.

with the influence of the Reynolds number. Physically, inertial forces enhance the consequences of Re and cause the lessening of the velocity curve. Figure 3 shows that the nanofluid velocity diminishes with the intensifying values of the magnetic factor, as the opposing force, that provides resistance in the flow direction generated due to the magnetic influence. That is why, the fluid velocity drops with the magnetic upshot as demonstrated in Figure 3. Figure 4 shows that the insertion of NPs in $C_2H_6O_2$ reduces the fluid velocity in the axial direction. Physically, the density of NPs is higher than $C_2H_6O_2$, and hence their dispersion makes the fluid density denser; as a result, fluid velocity drops as shown in Figure 4.

Figures 5–7 present the presentation of swirling curve $h(\eta)$ *versus* the Re, magnetic effect *M*, and NP volume friction, respectively. Figure 5 describes that the velocity distribution decays with the impact of the Reynolds number. Physically, the inertial forces enhance with the effect of Re, which results in the decrease of the momentum boundary layer. Figure 6 shows that the nanofluid velocity diminishes with the growing values of the magnetic factor because the resistive force provides resistance in the flow direction generated due to magnetic influence. Hence, the fluid velocity

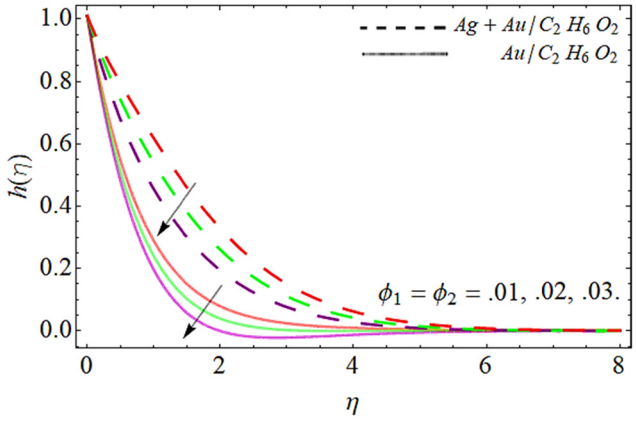

Figure 7: Performance of swirling curve $h(\eta)$ *versus* the NPs volume friction.

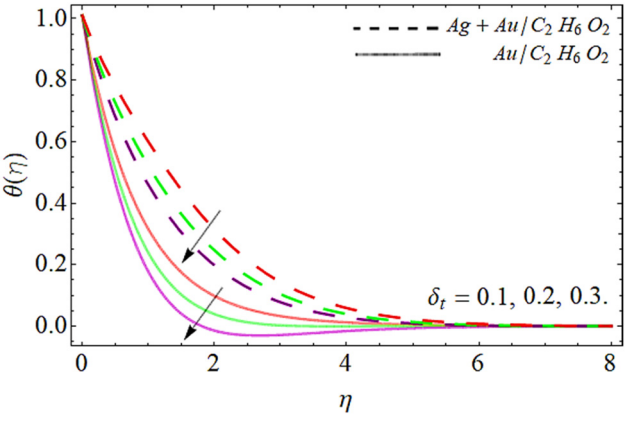

Figure 9: Performance of energy curve $\theta(\eta)$ *versus* the thermal relaxation factor δ_t.

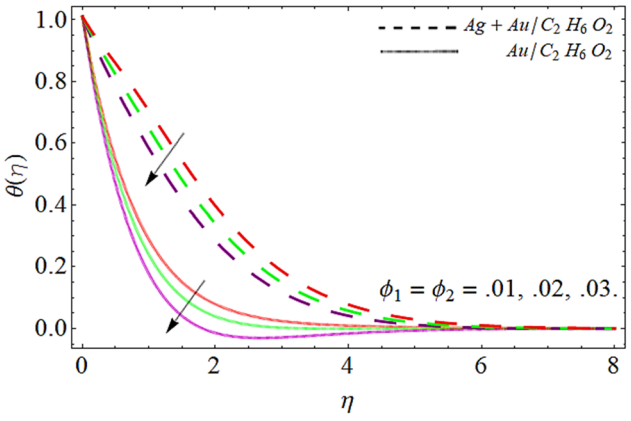

Figure 10: Performance of energy curve $\theta(\eta)$ *versus* the NPs volume friction.

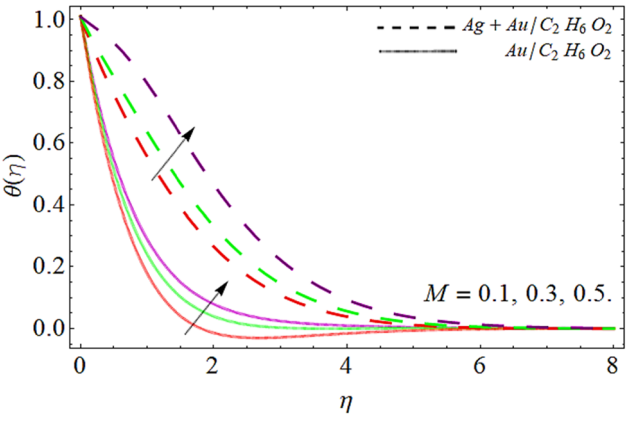

Figure 12: Performance of energy curve $\theta(\eta)$ *versus* the magnetic effect *M*.

drops with the magnetic upshot as demonstrated in Figure 6. Figure 7 shows that the inclusion of NPs in ethylene glycol reduces the fluid velocity in the radial direction. Physically, the density of Ag and Au NPs is higher than $C_2H_6O_2$, and hence, their scattering makes the fluid density denser and fluid velocity degenerates as shown in Figure 7.

4.2 Energy interpretation

Figures 8–12 illustrate the presentation of energy curve $\theta(\eta)$ *versus* the Re, thermal relaxation factor δ_t, NPs volume friction, heat source *H*, and magnetic effect *M*, respectively. Figures 8 and 9 express that the nanofluid energy outlines decrease with the influence of Reynolds number Re and thermal relaxation factor δ_t. As we have discussed ealier, interial forces boosts with the upshot of Re, which declines the energy curve as shown in Figure 8. Thermal relaxation time is the duration that it takes for an object to restore to its initial temperature after being heated. Hence, the rising

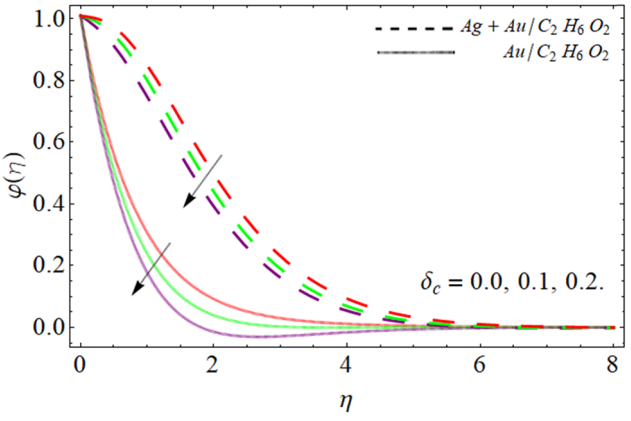

Figure 13: Performance of mass outline $\varphi(\eta)$ *versus* the solutal relaxation factor δ_c.

values of δ_t drops the nanofluid energy curve δ_t as shown in Figure 9. Figure 10 demonstrates that the temperature outlines also drop with the increasing numbers of Ag and Au NPs in the ethylene gylcol. Physcally, the thermal conductivity and

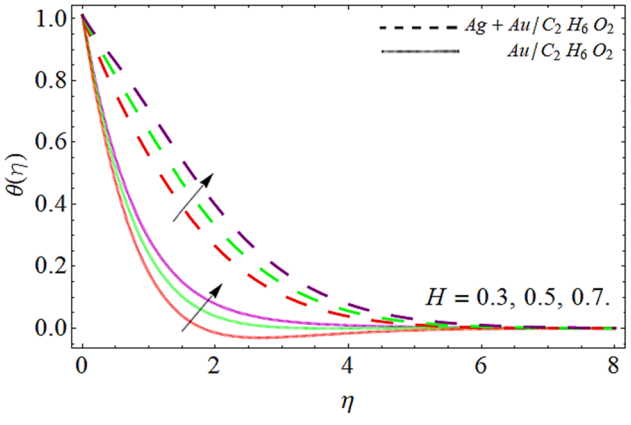

Figure 11: Performance of energy curve $\theta(\eta)$ *versus* the heat source *H*.

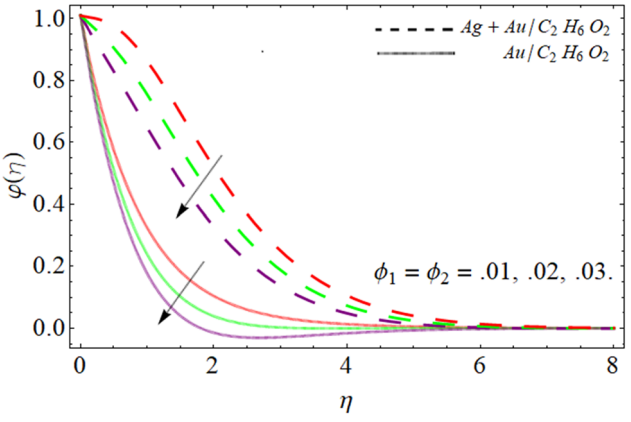

Figure 14: Performance of mass outline $\varphi(\eta)$ *versus* the NPs volume friction.

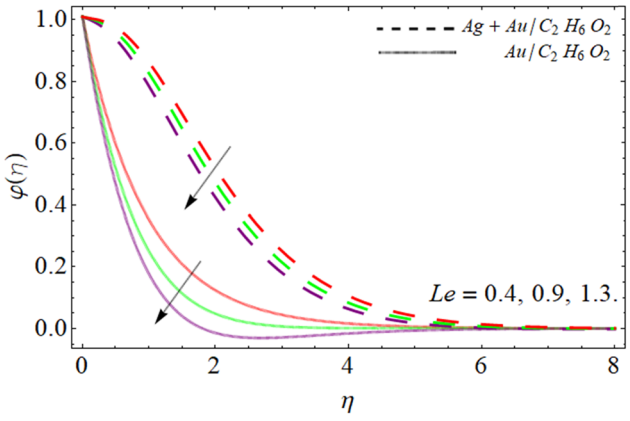

Figure 15: Performance of mass outline $\varphi(\eta)$ *versus* the Lewis number Le.

the density of nanoliquid increase with the addition of nano composities, which augments the energy-absorbing capability of the base fluid, as a result of a decrease in the fluid temperature δ_t. Figures 11 and 12 reveal that the nanofluid temperature outlines upsurges with the flourshing upshots of H (heat source) and magnetic field. During the chemical reaction, the atoms release some energy, which when added to the total energy of the fluid, causes inclination in the thermal profile as indicated in Figure 11. However, the resistive force that opposes the flow field also produces heat and ultimately the energy curve boosts as shown in Figure 12.

4.3 Mass interpretations

Figures 13–15 illustrate the presentation of mass outline $\varphi(\eta)$ *versus* the solutal relaxation factor δ_c, NPs volume friction, and Lewis number Le, respectively. Figures 13–15 demonstrate that the mass outlines decline with the influence of parameters δ_c, ϕ, and Le. Relaxation time is the period when a system relieves in response to external conditions that change. Hence, the action of the solutal relaxation factor descents the mass diffusion rate of nanofluid as shown in Figure 13. Likewise, the addition of Ag and Au NPs to base fluid makes the fluid atom denser, which causes the reduction of molecular diffusion rate, and thus, mass panel declines as shown in Figure 14. Figure 15 expresses that the mass distribution also weakens with the upsurge in the Lewis number. Table 3 reveals the statistical value for the Sherwood number, skin friction, and Nusselt number. Also, the skin friction enhances with the result of magnetic factor, while the energy transference rate declines.

Table 3: The statistical outputs for Sherwood number, skin friction, and Nusselt number

M	Re	$\phi_1 = \phi_2$	δ_t	$f''(1)$	$g'(1)$	$-\theta'(1)$	$-\varphi'(1)$
0.1	0.5	0.01	0.2	0.01382	3.66511	1.05166	0.83201
0.3				0.02744	3.89473	1.04799	0.83258
0.5				0.03924	4.10009	1.04508	0.83303
0.7				0.05090	1.75129	1.05648	0.83127
	0.5			0.05592	1.86606	1.17839	0.88044
	1.0			0.06103	1.98190	1.29760	1.01614
	1.5			0.06623	1.09873	1.41310	1.05927
	2.0			0.08745	3.40207	1.51518	1.70389
		0.01		0.08732	3.40205	1.36499	0.67873
		0.02		0.08723	3.40196	1.41399	0.65379
		0.03		0.08654	3.40178	1.50938	0.62171
		0.04		0.08645	3.40107	1.03834	0.58124
			0.2	0.08645	3.40206	1.03215	0.84004
			0.4	0.08542	3.40204	1.13743	0.88745
			0.6	0.08454	3.40123	1.27348	0.71823
			0.8	0.08245	3.40007	1.45929	0.70920

5 Conclusions

This study examined the heat and mass conveyance through the fluid flow across a swirling cylinder under the impact of magnetic effects and Cattaneo–Christov heat flux, heat source/sink, and reactive species. The hybrid nanoliquid has been produced by the dispersion of Ag and Au NPs in $C_2H_6O_2$ (pure fluid). The modeled equations are reduced to the dimensionless system of ODEs by employing the similarity substitution. For the numerical estimation of the problem, PCM methodology is used. The main findings are as follows:

- The axial velocity distribution drops with the impact of the Reynolds number, magnetic effect, and the inclusion of Ag and Au NPs in $C_2H_6O_2$.
- Nanofluid energy outlines decrease with upsurge Reynolds number Re, thermal relaxation factor δ_t, and the rising number of Ag and Au NPs.
- Swirling velocity outline also diminishes due to the effects of NPs volume friction, Reynolds number, and magnetic factor.
- Mass outlines drop with the flourishing values of solutal relaxation factor δ_c, NPs volume friction, and Lewis number Le.
- The temperature field upsurges for flourshing effects of heat source H and magnetic field.
- The present mathematical model can be modified to other types of fluid models and can also be numerically and analytically solved.

Acknowledgments: The authors acknowledge support from the Deanship of Scientific Research, the Vice Presidency for Graduate Studies and Scientific Research, King Faisal University, Saudi Arabia (Grant No. 5783).

Funding information: This work was supported by the Deanship of Scientific Research, the Vice Presidency for Graduate Studies and Scientific Research, King Faisal University, Saudi Arabia (Grant No. 5783).

Author contributions: All authors have accepted responsibility for the entire content of this manuscript and approved its submission.

Conflict of interest: The authors state no conflict of interest.

Data availability statement: All data generated or analysed during this study are included in this published article.

References

[1] Dufrane KF. Wear perfomance of ceramics in ring/cylinder applications. J Am Ceram Soc. 1989 Apr;72(4):691–5.
[2] Chu YM, Bashir S, Ramzan M, Malik MY. Model-based comparative study of magnetohydrodynamics unsteady hybrid nanofluid flow between two infinite parallel plates with particle shape effects. Math Methods Appl Sci. 2023 Jul 15;46(10):11568–82.
[3] Karlsson J, Fredriksson J. Cylinder-by-cylinder engine models *vs* mean value engine models for use in powertrain control applications. SAE Technical Paper; 1999 Mar 1.
[4] Bilal M, Saeed A, Selim MM, Gul T, Ali I, Kumam P. Comparative numerical analysis of Maxwell's time-dependent thermo-diffusive flow through a stretching cylinder. Case Stud Therm Eng. 2021 Oct 1;27:101301.
[5] Pattnaik PK, Abbas MA, Mishra S, Khan SU, Bhatti MM. Free convective flow of hamilton-crosser model gold-water nanofluid through a channel with permeable moving walls. Comb Chem High Throughput Screen. 2022 Jul 1;25(7):1103–14.
[6] Kumar RN, Gowda RP, Abusorrah AM, Mahrous YM, Abu-Hamdeh NH, Issakhov A, et al. Impact of magnetic dipole on ferromagnetic hybrid nanofluid flow over a stretching cylinder. Phys Scr. 2021 Feb 12;96(4):045215.
[7] Alhowaity A, Hamam H, Bilal M, Ali A. Numerical study of Williamson hybrid nanofluid flow with thermal characteristics past over an extending surface. Heat Transf. 2022 Nov;51(7):6641–55.
[8] Abbasi A, Farooq W, Tag-ElDin ES, Khan SU, Khan MI, Guedri K, et al. Heat transport exploration for hybrid nanoparticle (Cu, Fe_3O_4) —Based blood flow *via* tapered complex wavy curved channel with slip features. Micromachines. 2022 Aug 28;13(9):1415.
[9] Pattnaik PK, Mishra SR, Bég OA, Khan UF, Umavathi JC. Axisymmetric radiative titanium dioxide magnetic nanofluid flow on a stretching cylinder with homogeneous/heterogeneous reactions in Darcy-Forchheimer porous media: Intelligent nanocoating simulation. Mater Sci Eng B. 2022 Mar 1;277:115589.
[10] Ramzan M, Algehyne EA, Saeed A, Dawar A, Kumam P, Watthayu W. Homotopic simulation for heat transport phenomenon of the Burgers nanofluids flow over a stretching cylinder with thermal convective and zero mass flux conditions. Nanotechnol Rev. 2022 Apr 1;11(1):1437–49.
[11] Seid E, Haile E, Walelign T. Multiple slip, Soret and Dufour effects in fluid flow near a vertical stretching sheet in the presence of magnetic nanoparticles. Int J Thermofluids. 2022 Feb 1;13:100136.
[12] Umar M, Amin F, Al-Mdallal Q, Ali MR. A stochastic computing procedure to solve the dynamics of prevention in HIV system. Biomed Signal Process Control. 2022 Sep 1;78:103888.
[13] Reddy YD, Goud BS, Nisar KS, Alshahrani B, Mahmoud M, Park C. Heat absorption/generation effect on MHD heat transfer fluid flow along a stretching cylinder with a porous medium. Alex Eng J. 2023 Feb 1;64:659–66.
[14] Sreedevi P, Reddy PS. Flow and heat transfer analysis of carbon nanotubes based nanofluid flow inside a cavity with modified Fourier heat flux. Phys Scr. 2021;96(5).
[15] Sudarsana Reddy P, Sreedevi P. Impact of chemical reaction and double stratification on heat and mass transfer characteristics of nanofluid flow over porous stretching sheet with thermal radiation. Int J Ambient Energy. 2022 Dec 31;43(1):1626–36.
[16] Yu W, Xie H. A review on nanofluids: Preparation, stability mechanisms, and applications. J Nanomater. 2012 Jan 1;2012:1–7.
[17] Rauf A, Faisal, Shah NA, Botmart T. Hall current and morphological effects on MHD micropolar non-Newtonian tri-hybrid nanofluid flow between two parallel surfaces. Sci Rep. 2022 Oct 5;12(1):16608.
[18] Zhao J, Pinchuk AO, McMahon JM, Li S, Ausman LK, Atkinson AL, et al. Methods for describing the electromagnetic properties of silver and gold nanoparticles. Acc Chem Res. 2008 Dec 16;41(12):1710–20.
[19] Rónavári A, Igaz N, Adamecz DI, Szerencsés B, Molnar C, Kónya Z, et al. Green silver and gold nanoparticles: Biological synthesis approaches and potentials for biomedical applications. Molecules. 2021 Feb 5;26(4):844.
[20] Assiri TA, Aziz Elsebaee FA, Alqahtani AM, Bilal M, Ali A, Eldin SM. Numerical simulation of energy transfer in radiative hybrid nanofluids flow influenced by second-order chemical reaction and magnetic field. AIP Adv. 2023 Mar 1;13(3).
[21] Waqas H, Farooq U, Hassan A, Liu D, Noreen S, Makki R, et al. Numerical and computational simulation of blood flow on hybrid nanofluid with heat transfer through a stenotic artery: Silver and gold nanoparticles. Results Phys. 2023 Jan 1;44:106152.
[22] Bilal M, Saeed A, Gul T, Ali I, Kumam W, Kumam P. Numerical approximation of microorganisms hybrid nanofluid flow induced by a wavy fluctuating spinning disc. Coatings. 2021 Aug 27;11(9):1032.
[23] Alharbi KA, Ahmed AE, Sidi MO, Ahammad NA, Mohamed A, El-Shorbagy MA, et al. Computational valuation of Darcy ternary-hybrid nanofluid flow across an extending cylinder with induction effects. Micromachines. 2022;13:588.
[24] Zhang Y, Shahmir N, Ramzan M, Alotaibi H, Aljohani HM. Upshot of melting heat transfer in a Von Karman rotating flow of gold-silver/engine oil hybrid nanofluid with cattaneo–christov heat flux. Case Stud Therm Eng. 2021 Aug 1;26:101149.
[25] Akram J, Akbar NS, Tripathi D. A theoretical investigation on the heat transfer ability of water-based hybrid (Ag–Au) nanofluids and Ag nanofluids flow driven by electroosmotic pumping through a microchannel. Arab J Sci Eng. 2021 Mar;46:2911–27.
[26] Sreedevi P, Reddy PS, Suryanarayana Rao KV. Effect of magnetic field and radiation on heat transfer analysis of nanofluid inside a square cavity filled with silver nanoparticles: Tiwari–Das model. Waves Random Complex Media. 2021 Apr 28;1–9.

[27] Waqas H, Farooq U, Liu D, Alghamdi M, Noreen S, Muhammad T. Numerical investigation of nanofluid flow with gold and silver nanoparticles injected inside a stenotic artery. Mater Des. 2022 Nov 1;223:111130.
[28] Nanda P, Sandeep N, Sulochana C, Ashwinkumar GP. Enhanced heat transmission in methanol-based AA7072/AA7075 tangent hyperbolic hybrid nanofluid flow along a nonlinear expandable surface. Numer Heat Transfer Part A: Appl. 2023 Apr 3;83(7):711–25.
[29] Shahzad A, Liaqat F, Ellahi Z, Sohail M, Ayub M, Ali MR. Thin film flow and heat transfer of Cu-nanofluids with slip and convective boundary condition over a stretching sheet. Sci Rep. 2022 Aug 22;12(1):14254.
[30] Reddy PS, Sreedevi P, Suryanarayana Rao KV. Impact of heat generation/absorption on heat and mass transfer of nanofluid over rotating disk filled with carbon nanotubes. Int J Numer Methods Heat Fluid Flow. 2021 Aug 26;31(9):2962–85.
[31] Nazia S, Seshaiah B, Sudarsana Reddy P, Sreedevi P. Silver–ethylene glycol and copper–ethylene glycol based thermally radiative nanofluid characteristics between two rotating stretchable disks with modified Fourier heat flux. Heat Transf. 2023 Jan;52(1):289–316.
[32] Pattnaik PK, Parida SK, Mishra SR, Abbas MA, Bhatti MM. Analysis of metallic nanoparticles (Cu, Al2O3, and SWCNTs) on magnetohydrodynamics water-based nanofluid through a porous medium. J Math. 2022 Feb 14;2022:1–2.
[33] Baag S, Mishra SR, Hoque MM, Anika NN. Magnetohydrodynamic boundary layer flow over an exponentially stretching sheet past a porous medium with uniform heat source. J Nanofluids. 2018 Jun 1;7(3):570–6.
[34] Chandra Sekar Reddy R, Reddy PS, Sreedevi P. Impact of the Cattaneo–Christov heat flux on heat and mass transfer analysis of a hybrid nanofluid flow over a vertical cone. Int J Ambient Energy. 2022 Dec 31;43(1):6919–31.
[35] Bejawada SG, Nandeppanavar MM. Effect of thermal radiation on magnetohydrodynamics heat transfer micropolar fluid flow over a vertical moving porous plate. Exp Comput Multiph Flow. 2023 Jun;5(2):149–58.
[36] Bejawada SG, Reddy YD, Jamshed W, Nisar KS, Alharbi AN, Chouikh R. Radiation effect on MHD Casson fluid flow over an inclined non-linear surface with chemical reaction in a Forchheimer porous medium. Alex Eng J. 2022 Oct 1;61(10):8207–20.
[37] Kodi R, Mopuri O. Unsteady MHD oscillatory Casson fluid flow past an inclined vertical porous plate in the presence of chemical reaction with heat absorption and Soret effects. Heat Transf. 2022 Jan;51(1):733–52.
[38] Mahabaleshwar US, Vishalakshi AB, Hatami M. MHD micropolar fluid flow over a stretching/shrinking sheet with dissipation of energy and stress work considering mass transpiration and thermal radiation. Int Commun Heat Mass Transf. 2022 Apr 1;133:105966.
[39] Sadaf M, Arshed S, Akram G, Ali MR, Bano I. Analytical investigation and graphical simulations for the solitary wave behavior of Chaffee–Infante equation. Results Phys. 2023 Nov 1;54:107097.
[40] Ali KK, Yusuf A, Yokus A, Ali MR. Optical waves solutions for the perturbed Fokas–Lenells equation through two different methods. Results Phys. 2023 Oct 1;53:106869.
[41] Ali A, Ahammad NA, Tag-Eldin E, Gamaoun F, Daradkeh YI, Yassen MF. MHD Williamson nanofluid flow in the rheology of thermal radiation, Joule heating, and chemical reaction using the Levenberg–Marquardt neural network algorithm. Front Energy Res. 2022;1175.
[42] Adnan, Nadeem A, Mahmoud HA, Ali A, Eldin SM. Significance of Koo-Kleinstreuer-Li model for thermal enhancement in nanofluid under magnetic field and thermal radiation factors using LSM. Adv Mech Eng. 2023 Oct;15(10):16878132231206906.
[43] Pattnaik PK, Moapatra DK, Mishra SR. Influence of velocity slip on the MHD flow of a micropolar fluid over a stretching surface. In Recent trends in applied mathematics: Select Proceedings of AMSE 2019 2021. Singapore: Springer; p. 307–21.
[44] Nisar KS, Mohapatra R, Mishra SR, Reddy MG. Semi-analytical solution of MHD free convective Jeffrey fluid flow in the presence of heat source and chemical reaction. Ain Shams Eng J. 2021 Mar 1;12(1):837–45.
[45] Makinde OD, Mishra SR. Chemically reacting MHD mixed convection variable viscosity Blasius flow embedded in a porous medium. In Defect and Diffusion Forum 2017 May 31. Vol. 374, Trans Tech Publications Ltd; p. 83–91.
[46] Ahmed A, Khan M, Ahmed J. Thermal analysis in swirl motion of Maxwell nanofluid over a rotating circular cylinder. Appl Math Mech. 2020 Sep;41:1417–30.
[47] Ahmed J, Shahzad A, Farooq A, Kamran M, Ud-Din Khan S, Ud-Din Khan S. Thermal analysis in swirling flow of titanium dioxide–aluminum oxide water hybrid nanofluid over a rotating cylinder. J Therm Anal Calorim. 2021 Jun;144:2175–85.
[48] Shamshuddin MD, Mabood F, Bég OA. Thermomagnetic reactive ethylene glycol-metallic nanofluid transport from a convectively heated porous surface with Ohmic dissipation, heat source, thermophoresis and Brownian motion effects. Int J Model Simul. 2022 Sep 3;42(5):782–96.
[49] Fang T, Yao S. Viscous swirling flow over a stretching cylinder. Chin Phys Lett. 2011 Nov 1;28(11):114702.
[50] Berezowski M. The application of the parametric continuation method for determining steady state diagrams in chemical engineering. Chem Eng Sci. 2010 Oct 1;65(19):5411–4.
[51] Patil A. A modification and application of parametric continuation method to variety of nonlinear boundary value problems in applied mechanics. Rochester Institute of Technology; 2016.
[52] Algehyne EA, Alrihieli HF, Saeed A, Alduais FS, Hayat AU, Kumam P. Numerical simulation of 3D Darcy–Forchheimer fluid flow with the energy and mass transfer over an irregular permeable surface. Sci Rep. 2022 Aug 26;12(1):14629.
[53] Raizah Z, Saeed A, Bilal M, Galal AM, Bonyah E Parametric simulation of stagnation point flow of motile microorganism hybrid nanofluid across a circular cylinder with sinusoidal radius. Open Phys. 2023 Jan 25;21(1):20220205.